ACS OMEGA

Open Access

http://pubs.acs.org/journal/acsodf

Article

Self-Healing Conjugated Microporous Polyanilines for Effective and Continuous Catalytic Detoxification of 4-Nitrophenol to 4-Aminophenol

Weiming Gao, Dingwu Jiang, Yiming Zhang, Yao Li, Zhilong Xu, Runxi Han, Hao Tian, Hufei Dai, Qijing Lu, and Cuiping Li*

Cite This: *ACS Omega* 2024, 9, 11431−11442

Read Online

ACCESS | Metrics & More | Article Recommendations | Supporting Information

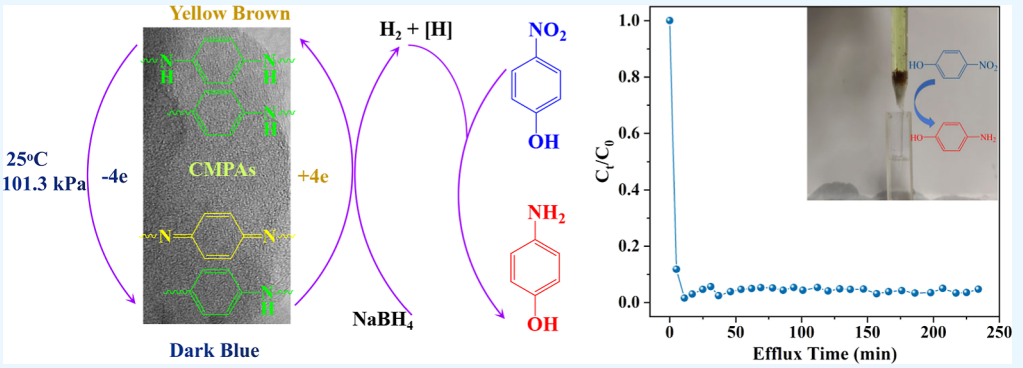

ABSTRACT: Detoxification of 4-nitrophenol (4-NP) to 4-aminophenol (4-AP) with high efficiency and dynamic performance is challenging for a polymeric catalyst. Herein, a series of conjugated microporous polyanilines (CMPAs), capable of efficiently catalytically reducing 4-NP, were synthesized based on the Buchwald−Hartwig cross-coupling reaction mechanism. By adjusting the types of linkers and the molar ratios of linker to core, CMPAs with different Brunauer−Emmett−Teller (BET) specific surface areas and reduction degrees were obtained and used as the catalysts in reducing 4-NP. The ultrahigh catalytic reduction efficiency (K = 141.32 s^{-1} g^{-1}, k_{app} = 0.00353 s^{-1}) was achieved when using CMPA-3-0.7 as the catalyst (prepared with 4,4′-diaminodiphenylamine as the linker and a 0.7:1 molar ratio of linker to core). The catalytic reduction performance exhibited a strong correlation with the reduction degree and BET specific surface area of CMPAs. Furthermore, they also exhibit excellent cycling stability and dynamic performance. The coexistence of a microporous structure and high BET specific surface area endowed CMPAs with an increased number of catalytic active centers. The reversible redox transformation of CMPAs in the presence of $NaBH_4$ and air enabled self-healing (the oxidation units in CMPAs were reduced to reduction units by $NaBH_4$, and the newly generated reduction unit in CMPAs was subsequently oxidized to its original state by the O_2 in the air), leading to the reduction reaction of 4-NP proceeded continuously and stably. The aforementioned factors resulted in the high efficiency of CMPAs for reducing 4-NP to 4-AP, enhancing the practical application prospects of CMPAs in the detoxification of 4-NP wastewater.

INTRODUCTION

4-Nitrophenol (4-NP) is a significant and detrimental contaminant in dye, pharmaceutical, and pesticide industries wastewater.[1] It can damage the nervous system and organs through bioaccumulation, thus endangering human health.[2] Therefore, various approaches have been developed and utilized to the detoxification of 4-NP wastewater,[3,4] including chemical redox[5] and bacterial remediation methods.[6] Among the chemical redox methods, catalytic hydrogenation is an attractive method because of its higher catalytic efficiency and the added value of catalytic hydrogenation products, [4-aminophenol (4-AP)] as important intermediates.[7−11] Although a variety of catalysts have been applied to the catalytic hydrogenation of 4-NP, metal-based nanocatalysts with different microstructures and sizes are extensively used and the supports for these metal-based nanoparticles are usually accompanied to avoid the aggregation of metal-based nanoparticles.[3,7−12] For example, mesoporous hydroxyapatite-supported carbon dots/copper oxide and 2D silica nanosheet-supported silver nanoparticles with $NaBH_4$ as a reducing agent

Received: October 9, 2023
Revised: January 8, 2024
Accepted: January 12, 2024
Published: March 4, 2024

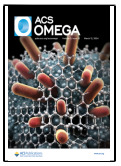

are used, resulting in K (activity parameter) values of 0.42 and 8.02 s^{-1} g^{-1}, respectively.[7,8]

On the flipside, the catalytic field has shown significant interest in polymers for their convenient chemical modification, resistance to corrosion, undemanding fabrication, as well as low-cost.[13−16] They are reported to exhibit catalytic capabilities that are on par with or surpass those of metal-containing catalysts. As an example, nano polyanilines (PANIs)[15] and halloysite nanotube-supported PANIs[16] with varying doping degrees have been directly used as catalysts to selectively oxidize cyclohexene with H_2O_2 as the oxidant in a solvent-free reaction system and have exhibited exceptional catalytic activity (k_w = 67.3 mmol g^{-1} h^{-1}, TON = 148.7 for halloysite nanotube supported PANIs). Moreover, formyl-modified PANIs and sulfonated PANIs have been used as solid base catalysts in the fructose dehydration to HMF.[17,18] The catalytic activities of PANIs are found to be correlated with their redox state, size, and degree of doping degree. Considering the presence of oxidation and reduction units in PANIs, they are employed to the catalytic reduction of 4-NP. Unfortunately, the catalytic reduction activities are almost negligible, despite utilizing various morphologies (such as microspheres, nanofibers, irregular shapes, and supported) of the emeraldine salt PANIs (Figure S1). Inspired by the observation that halloysite nanotube-supported PANIs can effectively electrostatically adsorb Cr (VI) oxyanion and simultaneously reduce it to Cr (III), but accompanied by an increase in oxidation degree, as well as the necessity for recovering supported PANIs,[19] the negligible catalytic activity of PANIs (emeraldine salts) for reducing 4-NP can potentially arise from their nonself-healing properties and low reduction degree (<50%). Moreover, in conjunction with the fact that porous polymeric catalysts typically demonstrate enhanced catalytic efficiency due to their high specific surface area and micropores/mesoporous structures,[20,21] it becomes crucial to synthesize PANIs possessing self-healing characteristics alongside a high reduction degree and BET specific surface area in order to address the issue of limited reduction efficiency exhibited by conventional PANI in catalytic reducing 4-NP.

The most widely applied synthesis method for PANIs with the aforementioned desired characteristics is the Buchwald−Hartwig (BH) coupling reaction. In this method, C−N bonds are constructed via the cross-coupling of aromatic halides and amines, forming a structure similar to that of PANIs, but having a π-conjugated three-dimensional (3D) network and microporous structure that is generally called conjugated microporous PANIs (CMPAs).[22−24] However, two significant drawbacks of this method are the low surface areas of CMPAs (*ca.* 50 m^2 g^{-1}) and low micropore volumes. These can be somewhat regulated by the variety of linker and core.[25] The addition of inorganic salts to a BH coupling reaction system can optimize and regulate the solvent's Hansen solubility parameter, thus giving a strong effect on the characteristics of the growing polymeric porous networks, making the pore size reduce to microporous dimension and finally resulting in a structure similar to MOF and COF and a substantial increase in the BET specific surface area from dozens m^2/g to more than 1000 m^2/g.[25−27] Because CMPAs synthesized by BH coupling reaction with an addition of inorganic salts have flexible π-conjugated 3D network, large surface area, adjustable pore structure, high chemical stability and reversible redox activity,[28] they are widely used in heterogeneous catalysis,[29] energy storage,[30,31] and heavy metal ion removal.[27,32] We believe that the utilization of CMPAs for catalytic reduction of 4-NP should have the following advantages over previously reported catalysts: (1) it will develop the application of polymers in catalytically reducing 4-NP; (2) the rich microporous structure as well as the high BET specific surface area (S_{BET}) of CMPAs will provide more catalytic active sites for reducing 4-NP, thus giving rise to an enhanced 4-NP reduction activity; (3) the reversible redox transition of CMPAs will avoid the deactivation of catalyst, giving rise to a superior dynamic reduction performance and cyclic stability, together with a practical application prospect in the detoxification of 4-NP wastewater. Although CMPAs have been used in Suzuki−Miyaura coupling reactions in the field of catalysis, they only act as the supports for palladium catalysts.[29] As far as we are aware, directly using CMPAs as the catalysts for 4-NP reduction, especially its superior catalytic activity (K = 141.32 s^{-1}·g^{-1}) and dynamic reduction performance, has never been reported.

In this work, CMPAs with varying S_{BET} and reduction degrees were synthesized by precisely controlling the types of linkers and their molar ratios to the core. Then, the relationship between the synthesis conditions (the types of linkers and the molar ratios of linker to core) and the catalytic performances of CMPAs in reducing 4-NP in terms of catalytic efficiency, cycling stability, and dynamic reduction capabilities was investigated. Finally, based on a comprehensive analysis of the structure-catalytic reduction activity in CMPAs, a mechanism was proposed elucidating how the reversible redox transformation of CMPAs promoted the decomposition of $NaBH_4$ and facilitated electron transfer during the 4-NP reduction process.

EXPERIMENTAL SECTIONS

Materials. Tris(4-bromophenyl)amine (98%) and XPhos (97%) were procured from Aladdin. *p*-Phenylenediamine (98%), NaO*t*Bu (99%), and $Pd(dba)_2$ (18.5% palladium) were procured from Adamas. 4,4′-Diaminodiphenylamine and tris(4-aminophenyl)amine were procured from Bide Medical Technology Co., Ltd. 4-NP (99%), $NaBH_4$ (98%), and NaF (98%) were respectively procured from China National Pharmaceutical Group Co., Ltd., Fuchen (Tianjin) Chemical Reagent Co., Ltd., and Jindong Tianzheng Fine Chemical Reagent Factory.

Synthesis of CMPAs. During the synthesis of CMPAs, three aromatic amines namely [tris(4-aminophenyl)amine, *p*-phenylenediamine and 4,4′-diaminodiphenylamine] were used as the linkers, and tris(4-bromophenyl)amine was used as the core.[27] The molar ratio of the linker to the core was 0.7:1. A typical process was as follows: 2.50 mmol core, 1.67 mmol linker, 0.225 mmol XPhos, 2.50 mmol NaF, 17.50 mmol NaO*t*Bu, 0.15 mmol $Pd(dba)_2$, and 150 mL dioxane were added to a flask with a magnetic stirrer. After being subjected to a series of sealing, repeatedly degassing/argon filling procedures, the flask was immersed in a thermostatic oil bath with a set temperature of 65 °C. After 48 h, the products were centrifuged and sequentially washed with chloroform ($CHCl_3$), methanol (MeOH), ethanol (EtOH), and boiling water (H_2O) first. Then, the mixture was subjected to Soxhlet extraction with $CHCl_3$, tetrahydrofuran (THF), and MeOH for 24 h each. After the drying process, three kinds of CMPAs were synthesized, which were respectively labeled as CMPA-1-0.7 [with tris(4-aminophenyl)amine as linker], CMPA-2-0.7 (with *p*-phenylenediamine as linker), and CMPA-3-0.7 (with 4,4′-

https://doi.org/10.1021/acsomega.3c07891
ACS Omega 2024, 9, 11431−11442

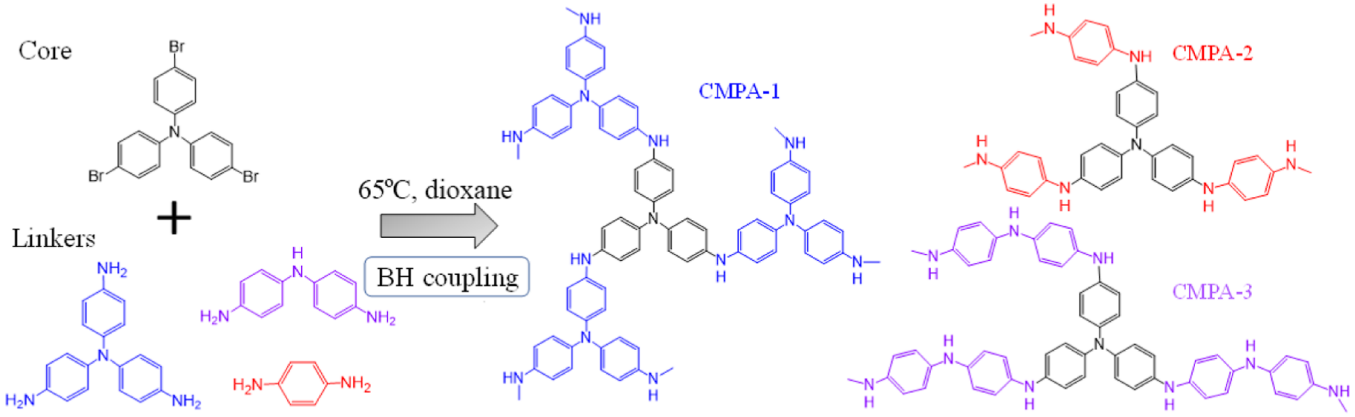

Figure 1. Synthetic route for CMPA networks through BH cross-coupling reaction between three aromatic amines and tri(4-bromophenyl)amine.

diaminodiphenylamine as linker). By a similar process, CMPA-3-Y with different molar ratios of linker to the core was also synthesized (Y = the molar ratio of linker to core).

Characterization. Fourier transform infrared (FT-IR) and solid UV−vis spectra were measured on a Thermo Nicolet 8700 spectrophotometer and a Hitachi U-4100 spectrometer, respectively. X-ray photoelectron spectroscopy (XPS) spectra were recorded on a Thermo Kalpha electron spectrometer (a Mono Al K_α source, 6 mA, 12 kV, and 1486.6 eV). X-ray diffraction (XRD) and thermogravimetric analysis (TGA) were respectively performed on a DX-2700B diffractometer (5−60° scan range, 10°/min scan rate) and Shimadzu TGA-50 (N_2 atmosphere, 10 °C/min heating rate). Transmission electron microscopy (TEM) and scanning electron microscopy (SEM) analysis were performed on JSM-2100 and Quanta 200 respectively. Nitrogen adsorption−desorption and UV−vis tests were, respectively, performed on Micromeritics ASAP 2460 (with samples degassed at 100 °C for 7 h) and UV1800PC. High-performance liquid chromatography (HPLC) characterization was carried on an Agilent 1100 (DAD detector, C18 column, mobile phase-30:70 of H_2O and CH_3CN).

4-NP Catalytic Reduction. The synthesized CMPAs were employed to catalyze 4-NP reduction using an excess of $NaBH_4$. The procedure typically unfolded as follows: first, 0.16 mL of a 1 mM aqueous solution of 4-NP, 2.0 mL of a 10 mM aqueous solution of $NaBH_4$, and 8 μL of a suspension containing CMPAs at a concentration of 2.5 mg/mL were introduced into a 10 mm quartz cell in sequence [(4-NP) = 0.0738 mM, ($NaBH_4$) = 9.225 mM]; subsequently, the reduction process of 4-NP was promptly tracked in real-time through UV−vis spectroscopy. For the test of cyclic stability, an additional 8 μL of a $NaBH_4$ solution with a concentration of 2.5 M and 8 μL of a 4-NP solution with a concentration of 20 mM were directly introduced into the reaction system without separation of catalyst from the reaction system and washing the catalyst. The dynamic experiment was carried out in a glass dropper with cotton wool sealing the narrower end. 9.5 mg CMPAs were weighed and put into the glass dropper. After that, a mixture of 10 mM $NaBH_4$/1 mM 4-NP solution, prepared at a 12.5:1 volume ratio, was continuously injected into the glass dropper at a certain flow rate (0.32 mL/min). The reaction effluents were monitored by UV−vis spectroscopy at certain time intervals.[12,33]

RESULTS AND DISCUSSION

Characterization of CMPAs Networks. CMPAs were synthesized based on a simple palladium-catalyzed BH cross-coupling reaction between three aromatic amine monomers and tri(4-bromophenyl)amine, which was an amination reaction used to generate C−N bonds (Figure 1). By this method, 3D conjugated networks with different redox activities were constructed by tuning the linker and the molar ratio of the linker to core. The addition of inorganic salts could optimize the pore structure of CMPAs and increase the specific surface area.[25−27] The synthesized CMPAs initially exhibited a yellow−brown color; however, with prolonged exposure to air, they underwent a gradual transformation into dark blue color, indicating the occurrence of air oxidation.

The synthesized CMPAs were first analyzed using solid UV−vis spectra, which confirmed the structure of PANI in CMPAs (Figure S2). For the CMPA-X-0.7 series (synthesized with a linker to core molar ratio of 0.7, but different types of linkers), they exhibited two broad peaks (240−440 nm assigned to the $\pi-\pi^*$ and π−polaron transitions in benzenoid rings, 440−800 nm associated with the polaron-π^* transitions in quinonoid rings).[16,19,34] The intensity ratio between these two peaks followed the order CMPA-3-0.7 > CMPA-2-0.7 > CMPA-1-0.7, implying that CMPA-3-0.7 possessed a greater abundance of benzenoid structures and the highest reduction degree. For the CMPA-3-Y series (fixed the linker as 4,4′-diaminodiphenylamine but different molar ratios of linker to core), the two broad peaks were gradually blue-shifted, and the peak intensity ratios decreased upon increasing the molar ratio of linker to core. The above results indicated the molar ratios of benzenoid structures to quinone structures or the redox state of CMPAs could be tuned by changing either the linker or the molar ratios of linker to core.

Furthermore, FTIR spectroscopy also proved the successful coupling between the linkers and cores as $-NH_2$ bond characteristic peaks of linkers at 3300/3400 cm^{-1} and C−Br bond stretching vibration peaks of the cores at 710, 1003, and 1072 cm^{-1} had disappeared in the spectra of CMPAs and were replaced with PANIs characteristic peaks (1257/1495 cm^{-1}—stretching vibrations of C−N/C═C bonds in the benzenoid structure, 1595 cm^{-1}—stretching vibrations of C═C bonds in the quinone structure) (Figure S3).[16,19,35] By comparing the peak intensities between 1495 and 1595 cm^{-1}, the reduction degree could be calculated and followed an order of CMPA-3-0.3 > CMPA-3-0.5 > CMPA-3-0.7 > CMPA-2-0.7 > CMPA-1-0.7 > CMPA-3−1 > CMPA-3-1.3 > CMPA-3-1.5. This

https://doi.org/10.1021/acsomega.3c07891
ACS Omega 2024, 9, 11431−11442

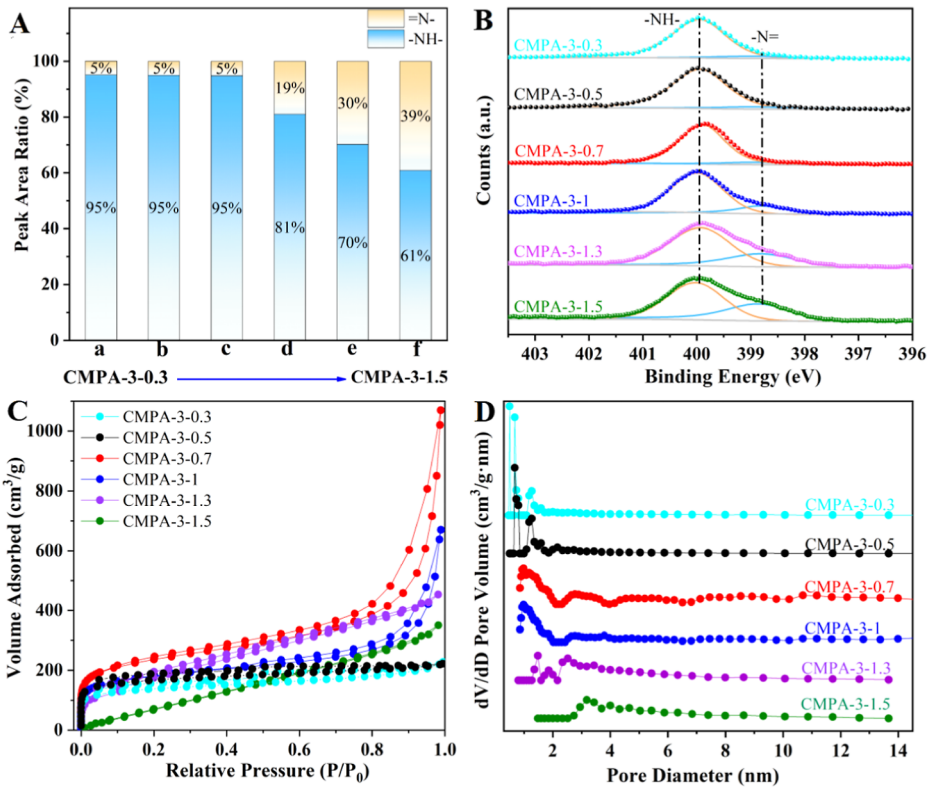

Figure 2. Peak area ratios for −NH− and =N− (A), N 1s high resolution spectra (B), nitrogen adsorption−desorption isotherm (C) and microporous/mesoporous pore size distribution [acquired based on the density functional theory (DFT) method] (D) of CMPA-3-Y.

sequence aligned with the outcomes obtained from solid UV−vis spectra analysis.

The redox states of the CMPA networks were further determined by XPS. The elementary compositions of CMPAs were C, N, and O atoms (Figure S4A). The intensity of the Pd 3d peak (335−340 eV) was negligible, indicating that a substantial proportion of the Pd^{2+} had been removed from the CMPAs by washing and Soxhlet extraction. In the N 1s high resolution spectra, two peaks were observed at approximately 398.8 eV (=N−) and 399.9 eV (−NH−), demonstrating the coexistence of N=Q=N (quinone structure) and N−B−N (benzenoid structure) bonds in the CMPA networks (Figures S4B and 2B).[36−38] For the −NH− and =N− peaks, the CMPA networks synthesized using different types of aromatic amine linkers had different area ratios and reduction degrees. The relative content of −NH− followed an order of CMPA-1-0.7 (93.26%) < CMPA-2-0.7 (93.90%) < CMPA-3-0.7 (94.85%) (Figure S4B and Table S1). The XPS spectra of CMPA-3-0.3, CMPA-3-0.5, CMPA-3-0.7, CMPA-3-1, CMPA-3-1.3, and CMPA-3-1.5 revealed that the molar ratio between the linker and core also affected the reduction degree (Figure 2A,B). When it was ≤0.7, the reduction degree of CMPA-3-Y held around 95%. Further increasing the dosage of 4,4′-diaminodiphenylamine reduced the −NH− relative content. The order of reduction degree for the CMPA-3-Y series was as follows: CMPA-3-0.3 (95.13%) > CMPA-3-0.5 (95.00%) > CMPA-3-0.7 (94.85%) > CMPA-3-1 (81.08%) > CMPA-3-1.3 (70.18%) > CMPA-3-1.5 (60.82%) (Figure 2A and Table S1). A combined result of solid UV−vis, FTIR, and XPS showed that CMPAs consisting of different amine/imine contents were constructed by adjusting either the linker or the molar ratio of the linker to core. The adjustable reduction degree and high S_{BET} of CMPAs, motivated us to study their selective catalytic hydrogenation performances for the conversion of 4-NP to 4-AP.

The crystalline structure of CMPAs was characterized by XRD. Unlike the crystalline structure of common COFs and MOFs, CMPA networks were amorphous (Figure S5). Moreover, CMPAs exhibited insolubility in commonly used organic solvents such as $CHCl_3$, CH_2Cl_2, MeOH, THF and dioxane, indicating their high chemical stability. The outstanding chemical stabilities of CMPAs derived from the highly cross-linked networks guaranteed their excellent catalytic durability in organic reactions. Besides, TGA results showed that the weight retentions of all the CMPA networks were higher than 88% at 300 °C. Among them, CMPA-3-0.7 demonstrated the highest thermal stability (83.47% weight retention at 800 °C) (Figure S6). In addition, the structures of CMPA-3-0.7 after being heated to 280 and 800 °C under a nitrogen atmosphere at a heating rate of 10 °C/min, respectively, denoted as CMPA-3-0.7-280 and CMPA-3-0.7-800, were also characterized by XPS. XPS exhibited the intensity of the N 1s peak decreased with the heating temperature, and the N contents of CMPA-3-0.7, CMPA-3-0.7-280 and CMPA-3-0.7-800 were 11.83, 8.96 and 6.66%, respectively. In addition, the relative content of −N= in CMPA-3-0.7-280 slightly increased from 5.15 to 6.79%, while that in CMPA-3-0.7-800 reached 17.36%, and an additional quaternary N peak located at 401.0 eV was appeared (Figure S7 and Table S1), indicating heating can result in the dehydrogenation of amine groups (−NH−) to imine group (−N=) and quaternary N.[39] The morphologies of the CMPAs were characterized by SEM and TEM. SEM images showed that CMPAs had a foam-like morphology, and the

https://doi.org/10.1021/acsomega.3c07891
ACS Omega 2024, 9, 11431−11442

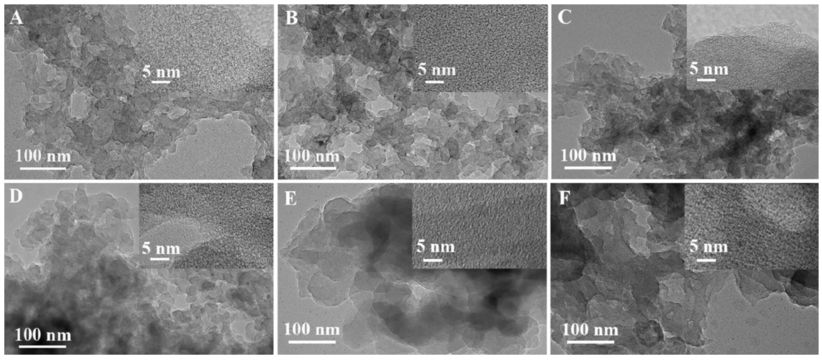

Figure 3. TEM images of CMPA-3-0.3 (A), CMPA-3-0.5 (B), CMPA-3-0.7 (C), CMPA-3-1 (D), CMPA-3-1.3 (E) and CMPA-3-1.5 (F).

polymer networks were connected by CMPA particles (Figure S8). TEM showed that CMPAs were microporous and uniform polymer particles (Figures 3 and S9). Upon increasing the linker's amount, agglomeration became more pronounced, and the observation of fine PANI particles became challenging when the molar ratio of linker to core exceeded 1:1, as exemplified by CMPA-3-1.3 and CMPA-3-1.5 (Figure 3E,F).

To further investigate the pore structure of CMPAs, nitrogen adsorption−desorption characterization was performed. According to the IUPAC classification, the adsorption−desorption isotherms of CMPAs, except that of CMPA-3-1.5, were defined as type I because their adsorption capacity increased rapidly at low relative pressures, indicating the presence of a typical microporous structure (Figures 2C and S10).[25] Furthermore, due to the interactions between fine polymer particles on the surface of CMPA networks, multilayer adsorption also occurred in a higher relative pressure range. The hysteresis loop at $P/P_0 > 0.5$ indicated the mesoporous characteristics of CMPAs. Figures 2D and S10B showed the microporous/mesoporous pore size distribution curves of different CMPA networks, from which almost all the CMPA networks, except CMPA-3-1.3 and CMPA-3-1.5, had both microporous and mesoporous structures and a high S_{BET} and micropore surface area (S_{micro}) (Table 1). Among them, CMPA-3-0.7 revealed the highest S_{BET} (870 m^2/g, including 432 m^2/g of S_{micro}), whereas CMPA-1-0.7 and CMPA-2-0.7 revealed lower S_{BET} values of 824 and 808 m^2/g (413 and 115 m^2/g of S_{micro}), respectively. These values were all much higher than those of bulk PANIs and supported PANIs.[16] In addition to the variety of linkers, the molar ratio of linker (4,4′-diaminodiphenylamine) to core also had a great impact on the pore structure. Upon increasing the dosage of linkers, S_{BET} exhibited a gradual increase from 498 m^2/g (CMPA-3-0.3) to 870 m^2/g (CMPA-3-0.7) initially, followed by a subsequent decrease to 384 m^2/g (CMPA-3-1.5). A similar trend was also observed for both S_{micro} and V_{micro} (micropore volume). For the samples synthesized at 1.3 and 1.5 molar ratios of linker to core, it was difficult to measure the S_{micro} and V_{micro}. The adsorption−desorption curves demonstrated that upon increasing the linker's quantity, the pore of CMPA-3-Y networks transitioned from predominantly microporous/mesoporous to intergranular pore. The intergranular pore could be attributed to the intricate macro- and mesostructures in samples.[40] The nitrogen adsorption−desorption results corresponded to the aggregation of polymer particles observed by TEM. We speculated that this phenomenon was caused by an incomplete coupling reaction due to the excessive or insufficient linker, which did not generate a complete conjugated 3D network, thus significantly reducing the microporous structure. Additionally, the impact of heating on its pore structure was also investigated, considering that it would lead to the dehydrogenation of amine groups (−NH−) into imine groups (−N═) and quaternary N (Figure S7B) at high temperature (800 °C). It disclosed that the S_{BET} of CMPA-3-0.7 after heating exhibited a slight decrease, decreasing from 870 to 830 m^2/g, whereas both the S_{micro} and V_{micro} witnessed a significant decrease (Table 1 and Figure S11), indicating heating to a high temperature of 800 °C had a limited effect on the S_{BET}, while it resulted in a decrease in the S_{micro} and V_{micro} owing to the dehydrogenation of amine groups.[39]

Table 1. Porosity Parameters of the CMPA Networks

	S_{BET}[a] (m^2/g)	S_{micro}[b] (m^2/g)	V_{micro}[b] (cm^3/g)	V_{tot}[c] (cm^3/g)
CMPA-1-0.7	824	413	0.179	1.097
CMPA-2-0.7	808	115	0.064	0.567
CMPA-3-0.3	498	330	0.141	0.276
CMPA-3-0.5	631	364	0.167	0.273
CMPA-3-0.7	870	432	0.184	1.149
CMPA-3-1	645	369	0.159	0.675
CMPA-3-1.3	621			0.702
CMPA-3-1.5	383			0.542
CMPA-3-0.7 (after catalysis)	849	416	0.177	1.162
CMPA-3-0.7-280	822	291	0.056	0.873
CMPA-3-0.7-800	830	346	0.000	0.592

[a]S_{BET} is the BET specific surface area. [b]S_{micro} and V_{micro} are the micropore surface area and micropore volume, respectively, and calculated based on the *t*-plot method. [c]V_{tot} is the total pore volume acquired based on the DFT method.

Catalytic Activity of CMPA Networks for Reducing 4-NP to 4-AP. The rich microporous structure and tunable redox properties of the CMPA networks motivated us to employ them to catalytically reduce 4-NP. The thermodynamic feasibility of 4-NP reduction has been well established, since the electrode potential of the 4-NP/4-AP pair is higher than that of H_3BO_3/BH_4^- pair over 0.57 V.[8,12] However, the dynamic feasibility of it is almost entirely limited without a catalyst. Herein, the catalytic performance of the CMPAs was evaluated through the 4-NP reduction reaction utilizing excessive amount of $NaBH_4$, and the reaction products were monitored by a UV1800PC. As shown in Figure 4A, both reactants and products had specific absorption peaks in a 250−500 nm wavelength range. The maximum absorption peak of the initial aqueous solution of 4-NP was observed at a

https://doi.org/10.1021/acsomega.3c07891
ACS Omega 2024, 9, 11431−11442

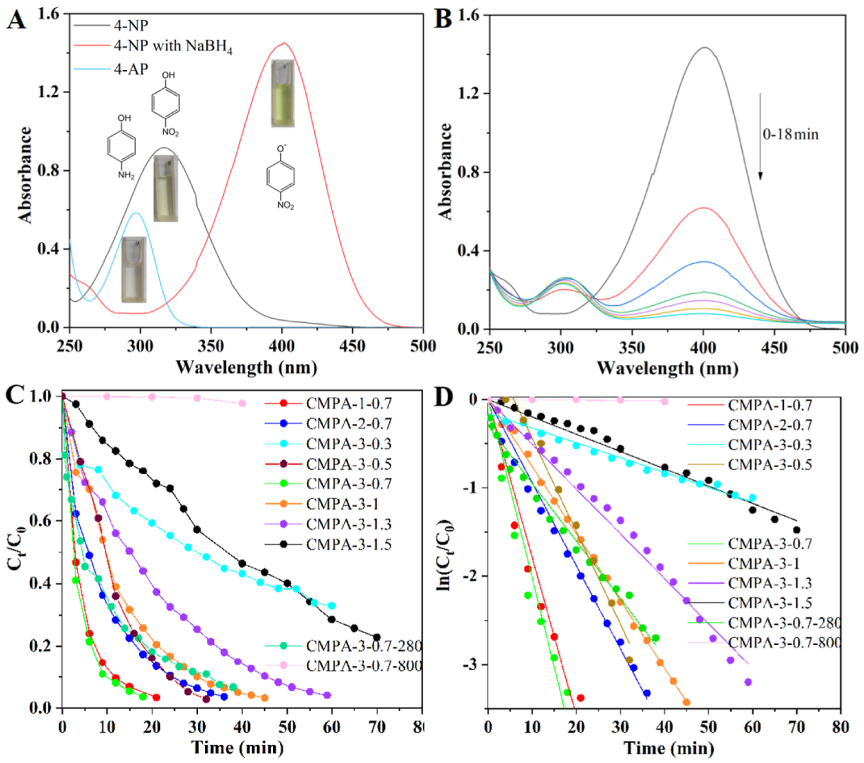

Figure 4. UV−vis spectra of reactant/product standards (A), and 4-NP reduction catalyzed by CMPA-3-0.7 (B); the correlation between C_t/C_0 and t (C) and the relationship between $\ln(C_t/C_0)$ and t (D) in the 4-NP reduction with CMPA networks as catalysts.

wavelength of 317 nm. Upon addition of $NaBH_4$, the 4-NP solution underwent a conspicuous color transition from pale yellow to vibrant yellow (Figure 4A), accompanied by a redshift in the UV−vis absorption spectra from 317 to 400 nm, indicating the ionization of 4-NP.[12] After completion of the reduction reaction, the resulting solution exhibited a colorless appearance with a prominent absorbance at 300 nm (ascribed to 4-AP). Given the more pronounced decrease in the absorption peak of 400 nm compared with the observed increase in 300 nm, this reduction reaction was primarily tracked by the decrease in the absorption peak of 400 nm.

The UV−vis spectra of 4-NP reduction with an excess quantity of $NaBH_4$ catalyzed by the series of CMPA-X-0.7 and CMPA-3-Y were shown in Figures 4B and S12. Figure S12A shows that the absence of CMPAs resulted in an insignificant decrease in the concentration of 4-NP, even after an extended reaction time of 24 h. However, in the presence of CMPAs, the absorbance of the 4-NP ion at 400 nm exhibited a continuous decrease with increasing reaction time, accompanied by a gradual enhancement of the peak at 300 nm (Figures 4B and S12B−H). Many bubbles were generated in the reaction solution. Finally, the reaction solution gradually turned colorless, illustrating 4-NP had been completely reduced without any detectable byproducts.[9,11] Among the CMPA-X-0.7 series, synthesized using the same core and molar ratio of linker to core but varying linkers, CMPA-3-0.7 demonstrated superior catalytic activity (Figure 4B) (completion of reaction within 18 min), followed by CMPA-1-0.7 (Figure S12B, completion of reaction within 21 min) and CMPA-2-0.7 (Figure S12C, completion of reaction within 36 min). The catalytic activity of CMPA-X-0.7 was positively correlated with S_{BET} and the relative content of −NH− in CMPAs. Furthermore, the catalytic activity of $Pd(dba)_2$ (the same dosage as that of CMPAs) for catalytic reducing 4-NP was also studied. It showed that the concentration of 4-NP remained unchanged even after 60 min, indicating that the catalytic activity of $Pd(dba)_2$ was negligible (Figure S13A). Therefore, the catalytic activity of CMPAs stemmed from themself, rather than the negligible amount of Pd^{2+} on CMPAs.

To further substantiate the correlation between the reduction degree/S_{BET} and the catalytic performance of CMPAs for reducing 4-NP, the catalytic activity of CMPA-3-Y (synthesized using the same core and linker but varying molar ratios of linker to core) was also investigated. When Y ≤ 0.7, the higher the molar ratio of linker to core, the shorter the reaction time required to complete the reduction reaction. For example, >60, 28 and 18 min were respectively needed when using CMPA-3-0.3, CMPA-3-0.5 and CMPA-3-0.7 as catalysts (Figures 4B and S12D,E). When Y > 0.7, the higher the molar ratio of linker to core, the longer the reaction time required to complete the reduction reaction. For example, 18, 45, 59, and >70 min were respectively needed when using CMPA-3-0.7, CMPA-3-1, CMPA-3-1.3, and CMPA-3-1.5 as catalysts (Figures 4B and S12F−H). Additionally, the impact of thermal treatment on the catalytic performance of CMPA-3-0.7 toward 4-NP reduction was also investigated. It was significant for CMPA-3-0.7-280 °C, the time required to complete the catalytic reduction was significantly prolonged from 18 to 38 min; whereas that for CMPA-3-0.7-800 was largely in excess of 40 min (Figure S14). As discussed above, since thermal treatment had less effect on the S_{BET} (Table 1), but decreased the reduction degree (−NH− relative content) (Table S1 and Figure S7B), the decrease in catalytic reduction activity of CMPA-3-0.7 after thermal treatment was largely dependent on the reduction degree. The above experimental results indicated that CMPAs had excellent thermal stability, high specific

https://doi.org/10.1021/acsomega.3c07891
ACS Omega 2024, 9, 11431−11442

Table 2. Comparative Analysis of Catalytic Activities Among CMPAs for Reducing 4-NP

samples	form	k_{app} (s^{-1})	K (s^{-1} g^{-1})	ref.
CMPA-1-0.7	3D network	0.00313	125.19	this work
CMPA-2-0.7	3D network	0.00159	63.70	this work
CMPA-3-0.3	3D network	0.00028	11.22	this work
CMPA-3-0.5	3D network	0.00176	70.23	this work
CMPA-3-0.7	3D network	0.00353	141.32	this work
CMPA-3-1	3D network	0.00128	51.06	this work
CMPA-3-1.3	3D network	0.00056	34.28	this work
CMPA-3-1.5	3D network	0.00034	13.44	this work
CMPA-3-0.7-280	3D network	0.00109	43.60	this work
CMPA-3-0.7-800	3D network	0.00001	0.40	this work
CMPA-3-0.7 without air	3D network	0.00012	4.80	this work
$Pd(dba)_2$		0	0	this work
$MnO@Al_2O_3@C/Ni$-700[a]	nanoflakes	0.00537	13.7	42
SiO2@C−Ni[a]	core−shell	0.00520	37	43
Au@CMK-3-O[b]	nanoparticles	0.00487	0.0065	44
Pt@Ag nanoparticles[c]	core−shell	0.00592	118.33	45
Pd−Ni alloy[d]	nanocomposite	0.00917	45.85	46

[a]Reaction condition: not be given. [b]Reaction condition: 75 mg Au@CMK-3-O, [$NaBH_4$] = 60 mM, [4-NP] = 1.43 mM. [c]Reaction condition: 50 μg Pt@Ag NPs, [$NaBH_4$] = 0.0089 mM, [4-NP] = 0.089 mM. [d]Reaction condition: 200 μg Pd−Ni alloy, [$NaBH_4$] = 3.75 mM, [4-NP] = 4.38 mM; Reaction condition: 20 μg CMPAs, [$NaBH_4$] = 9.225 mM, [4-NP] = 0.0738 mM.

surface area, and significant catalytic activity after undergoing thermal treatment at low temperature (280 °C). The reduction activity of CMPAs, however, was found to be negligible after undergoing thermal treatment at high temperature (800 °C) as the reduction degree of CMPAs experienced a substantial decrease.

The catalytic reduction activities of CMPAs were consistent with their reduction degree and S_{BET}. A high S_{BET} provided more catalytically active centers and increased the contact area between 4-NP and catalyst, thus improving the catalytic activity. The reason why a high reduction degree resulted in a high catalytic reduction activity will be discussed in the section of "4-NP reduction mechanism of CMPAs". Therefore, the catalytic performance of CMPAs networks toward reducing 4-NP by $NaBH_4$ was due to the combined effect of reduction degree and S_{BET}. Based on the aforementioned findings, it can be inferred that both the types of linkers, the molar ratio of linker to core, and the thermal treatment temperature during CMPAs preparation exerted an influence on the structure of CMPAs (reduction degree and S_{BET}), consequently affecting their catalytic reduction properties.

The products of 4-NP reduction were further analyzed by ^{1}H NMR and HPLC techniques. The ^{1}H NMR of the reaction products (treated by filtering and freeze-drying) toward CMPA-3-0.7 catalytically reducing 4-NP were shown in Figure S15. The characteristic proton signals of 4-AP (4.36, 6.48−6.36 ppm) were distinctly observed, consistent with the standard ^{1}H NMR spectrum of 4-AP.[12] In conjunction with the absence of characteristic proton signals of 4-NP (6.959 and 8.139 ppm), it could be inferred that a complete reduction of 4-NP to 4-AP had occurred. Moreover, this reaction product was characterized by HPLC (Figure S16). When 4-NP was reduced with CMPA-3-0.7 as a catalyst, it showed a peak near an elution time of 3.870 min, corresponding to 4-AP (an elution time of 3.848 min) (Figure S16B) without any 4-NP remnant (an elution time of 4.908 min). This observation also suggested the complete reduction of 4-NP to 4-AP. The conclusions drawn from the ^{1}H NMR and HPLC results aligned with those obtained from UV−vis spectroscopy (Figure 4B). Considering the validity, convenience of UV−vis analysis, as well as this reaction's rapidness, UV−vis spectroscopy was directly employed to monitor the reaction in the following section.

In the CMPAs catalyzing 4-NP reduction, the initial molar concentration of $NaBH_4$ exceeded that of 4-NP by a factor of 124 (9.225 mM vs 0.0738 mM). Therefore, the reduction reaction could be expressed by the following equation (C_t = [4-NP]$_t$, C_0 = [4-NP]$_0$, t was the reaction time).[41]

$$\ln\left(\frac{C_t}{C_0}\right) = -k_{app}t$$

Figure 4C showed the relationship between C_t/C_0 and t. It could be seen from the graph that CMPA-3-0.7 had the highest catalytic performance (C_t/C_0 dropped to zero within 18 min), and CMPA-3-0.7-800 exhibited the lowest catalytic activity (C_t/C_0 remained constant over a period of 40 min). Figure 4D demonstrates the correlation between $\ln(C_t/C_0)$ and t, which showed a robust linear correlation with the first-order reaction kinetics. Therefore, k_{app} could be derived by calculating the slope of $\ln(C_t/C_0)$ vs t. Furthermore, the catalytic activities of CMPAs were also assessed by the activity parameter K (K = k_{app}/the mass of catalyst). The k_{app} and K values were summarized in Table 2. It was obvious the catalytic efficiency of CMPAs toward 4-NP reduction was significantly influenced by the types of linkers and the molar ratios of linker to core as well as the thermal treatment temperature during their synthesis. Among them, CMPA-3-0.7 exhibited a maximum K of 141.32 s^{-1} g^{-1} and k_{app} of 0.00353 s^{-1}, followed by CMPA-1-0.7 (K = 125.19 s^{-1} g^{-1}, k_{app} = 0.00313 s^{-1}), CMPA-3-0.5 (K = 70.23 s^{-1} g^{-1}, k_{app} = 0.00176 s^{-1}), CMPA-2-0.7 (K = 63.70 s^{-1} g^{-1}, k_{app} = 0.00159 s^{-1}), CMPA-3-1 (K = 51.06 s^{-1} g^{-1}, k_{app} = 0.00128 s^{-1}), CMPA-3-0.7-280 (K = 43.60 s^{-1} g^{-1}, k_{app} = 0.00109 s^{-1}), CMPA-3-1.3 (K = 34.28 s^{-1} g^{-1}, k_{app} = 0.00056 s^{-1}), CMPA-3-1.5 (K = 13.44 s^{-1} g^{-1}, k_{app} = 0.00034 s^{-1}), CMPA-3-0.3 (K = 11.22 s^{-1} g^{-1}, k_{app} = 0.00028 s^{-1}), CMPA-3-0.7-800 (K = 0.40 s^{-1} g^{-1}, k_{app} = 0.00001 s^{-1}) and $Pd(dba)_2$ (K = 0 s^{-1} g^{-1}, k_{app} = 0 s^{-1}).

https://doi.org/10.1021/acsomega.3c07891
ACS Omega 2024, 9, 11431−11442

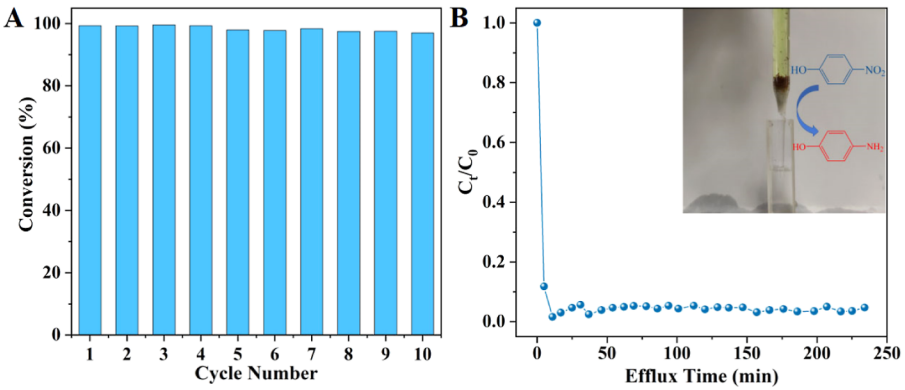

Figure 5. Reusability (A) and dynamic catalytic reduction performance (B) of CMPA-3-0.7.

With the comparable S_{BET}, the catalytic reduction activity of CMPAs exhibited an increase as the reduction degree was elevated (the CMPA-3-0.7-Z series). With a similar reduction degree, the catalytic reduction activity of CMPAs increased upon increasing the S_{BET} (the CMPA-X-0.7 and CMPA-3-Y series, Y ≤ 0.7). The catalytic activity of CMPA-3-0.7 for 4-NP reduction was comparable to and even outperformed some transition metal and noble metal-based catalysts (lines 13−17 in Table 2).[42−46] For example, K for MnO@Al_2O_3@C/Ni-700,[42] SiO_2@C-Ni,[43] Au@CMK-3-O,[44] Ag@Pt nanoparticles[45] and Pd−Ni alloy[46] catalyzing 4-NP reduction were 13.7, 37, 0.0065, 118.3 and 45.85 s^{-1} g^{-1}, respectively. All of these values were lower than the value obtained from CMPA-3-0.7 catalyzing 4-NP reduction, even though our reaction system had a higher concentration of 4-NP per unit mass of catalyst compared to the majority of other catalytic systems. The catalytic reduction performance of CMPA-3-0.7 was also found to surpass that of other PANI-based catalysts (prepared with aniline as monomer and ammonium persulfate as an oxidant) (Figure S1). As shown in Figure S1, no significant decrease in the 4-NP concentration was observed even at a longer reaction time of 60 min. We speculated that the enhanced catalytic reduction performance of CMPA-3-0.7 was ascribed to its high reduction degree and S_{BET}.

Reusability and Dynamic Catalytic Reduction Performance of CMPA. The reusability of catalysts is crucial for their commercial applications.[12,16] Compared with bulk or supported PANI materials, CMPAs had a more stable conjugated network structure and a higher reduction degree. Here, we chose CMPA-3-0.7 for reusability experiments (Figure 5A). The near-complete conversion was achieved after each cycle. Even after 10 cycles, over 97% of the initial catalytic efficiency was maintained, illustrating its excellent catalytic activity and reusability. The high S_{BET} and dense microporous structure provided an abundance of active centers for efficient electron transfer. The flexible redox transition of CMPAs may have also contributed to this, which will be further discussed in a subsequent section.

To demonstrate the practical applications of CMPA-3-0.7, a dynamic reduction test was conducted. A mixture of 10 mM $NaBH_4$/1 mM 4-NP solution, prepared at a 12.5:1 volume ratio, was continuously injected into a glass dropper with the catalyst immobilized by skimmed cotton at a specific flow rate (0.32 mL/min).[12] At specific time intervals, 3 mL of effluent was collected and subjected to UV−vis analysis to determine the residual concentration of 4-NP. As shown in the inset of Figure 5B, the mixed solution of 4-NP and $NaBH_4$ added to a glass dropper was stable and yellow before the reaction. Bubbles were generated upon the passage of the mixed solution through the immobilized catalyst, and the effluent solution became colorless, implying the complete reduction of 4-NP to 4-AP. The relationship between the effluent C_t/C_0 and t was demonstrated in Figure 5B, and the results showed that the reduction reaction maintained a high conversion of 4-NP and stable catalytic performance for at least 234 min. This contrasted with etched halloysite nanotubes@α-Ni$(OH)_2$ catalyzing 4-NP reduction[12] and halloysite nanotube-supported PANI (Figure S17). During the reaction, the catalyst exhibited a color change from dark blue to yellow within 2 min upon addition of the mixed solution of 4-NP and $NaBH_4$ (Figure S18A). After the reaction, blowing air into the glass dropper rapidly changed the catalyst's color to dark blue, similar to the phenomenon observed during CMPAs synthesis. When 9.5 mg of CMPA-3-0.7, CMPA-3-1, CMPA-3-1.3, and CMPA-3-1.5 was, respectively, added to centrifuge tubes containing 4 mL of $NaBH_4$ (10 mM) aqueous solution, they formed suspensions (Figure S18B). The colors of CMPA-3-0.7 and CMPA-3-1 immediately transitioned to yellowish brown, while those of CMPA-3-1.3 and CMPA-3-1.5 remained dark blue. After several hours, the colors of CMPA-3-0.7 and CMPA-3-1 reverted to dark blue, whereas those of CMPA-3-1.3 and CMPA-3-1.5 gradually transitioned into yellowish brown and ultimately returned to the original dark blue color upon complete decomposition of $NaBH_4$ in the suspensions. The observed phenomenon suggested that CMPAs can undergo reversible conversion between a benzenoid structure and a quinone structure in an aqueous solution of $NaBH_4$ (10 mM). In the aqueous solution of $NaBH_4$, the quinone unit in CMPAs underwent conversion to a benzenoid unit, leading to the release of H_2 or other [H] active species through $NaBH_4$ decomposition. This promoted catalytically reducing 4-NP to 4-AP. The reduced benzenoid unit in CMPAs was subsequently transformed into a quinone unit through oxidation by oxygen and air present in the solution, thereby facilitating structural self-repair.

4-Nitrophenol Reduction Mechanism of CMPAs. It was essential to explore why CMPAs prepared with different linkers and linker/core molar ratios showed different catalytic reduction activities. We first explored the points of their adsorption to 4-NP and 4-AP. Figures S19 and S20 showed that CMPAs exhibited varying adsorption capacities for 4-NP and 4-AP, following an order of CMPA-3-0.7 > CMPA-1-0.7 > CMPA-2-0.7 > CMPA-3-1 > CMPA-3-1.3 > CMPA-3-1.5. This order consistently corresponded to their catalytic

https://doi.org/10.1021/acsomega.3c07891
ACS Omega 2024, 9, 11431−11442

efficiencies in reducing 4-NP, thereby highlighting a positive correlation between catalytic activity and adsorption capacity. Thus, an elevated adsorption capacity toward 4-NP would facilitate the electron transfer between 4-NP and CMPAs, thus enhancing 4-NP reduction.

From the above discussion, the catalytic reduction performances of CMPAs were in accordance with their adsorption capacity toward 4-NP. This, in turn, was closely associated with the −NH− relative content and S_{BET} of CMPAs. For CMPA-X-Y series, CMPA-3-0.7 with the greatest −NH− relative content and S_{BET} (94.85%, Figure 2A and Table S1; 870 m^2/g, Entry 5, Table 1) showed the highest adsorption capacity toward 4-NP and catalytic efficiency in reducing 4-NP (K = 141.32 s^{-1} g^{-1}, Entry 5, Table 2). In contrast, CMPA-3-1.5 with the lowest −NH− relative content and S_{BET} (60.82%, Figure 2A and Table S1; 383 m^2/g, Entry 8, Table 1) exhibited the lowest adsorption capacity for 4-NP and catalytic efficiency in reducing 4-NP (K = 13.44 $s^{-1}\cdot g^{-1}$, Entry 8, Table 2). The samples exhibiting minimal variation in their −NH− relative content and S_{BET} were found to be comparable in catalytically reducing 4-NP (Entries 1, 2, 5, Table S1; Entries 1, 2, 5, Table 1; Entries 1, 2, 5, Table 2). Therefore, a higher surface area corresponded to an increased adsorption capacity toward 4-NP and enhanced catalytic activity because of more catalytic active centers and a higher contact area between 4-NP/$NaBH_4$ and catalyst.

To examine the effect of the −NH− relative content (reduction degree), CV measurements of CMPA-X-Y in the same concentration of $NaBH_4$ solution were conducted. The results were presented in Figure 6. The anodic peak current/

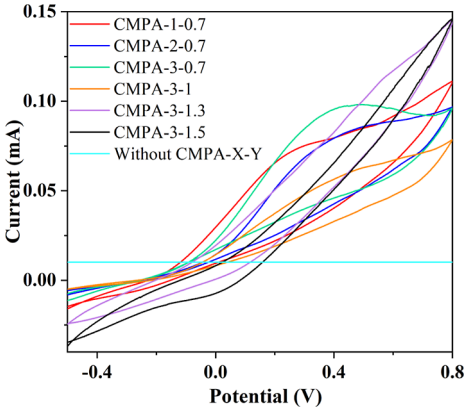

Figure 6. CV curves of the fabricated CMPAs (5 mg) in 30 mL of 10 mmol/L $NaBH_4$ solution (scan rate = 50 mV s^{-1}).

reduction potential of CMPA-3-0.7 was the highest among the CMPA-X-Y samples, indicating its easy electron transfer. The order was CMPA-3-0.7 > CMPA-2-0.7 > CMPA-1-0.7 > CMPA-3-1 > CMPA-3-1.3 > CMPA-3-1.5. The oxidation peak exhibited a gradual attenuation, while the reduction peak demonstrated a progressive enhancement in this sequence. For example, CMPA-3-0.7 exhibited only an oxidation peak, and CMPA-3-1.5 presented only a reduction peak. Considering the absence of any anodic peak without CMPA-X-Y, we could conclude that CMPA-3-0.7 was more readily oxidized to oxidized CMPAs, whereas CMPA-3-1.5 was more easily reduced to reduced CMPAs. This was consistent with the rate of the color change from yellow to dark blue (Figure S18). It was reasonable that a higher amine content increased the reduction degree, which provided the catalyst with a higher reduction potential and reducibility. This, in turn, facilitated the rapid transfer of electrons and the conversion of reduced CMPAs to oxidized CMPAs. Then, due to the excess amount of $NaBH_4$, oxidized CMPAs was reduced to reduced CMPAs, which was accompanied by the release of H_2 and reducing 4-NP to 4-AP.

In conjunction with the experimental findings, the color cycled from dark blue-yellowish brown in $NaBH_4$ solution (Figures 5B and S18), the enhanced oxidation peak of CMPA-3-0.7, a strong correlation between S_{BET}/reduction degree and the catalytic efficiency of CMPAs, a mechanism toward CMPAs catalytically reducing 4-NP was proposed (Scheme 1). First, the catalyst surface was adsorbed by 4-NP and BH_4^-

Scheme 1. Proposed Catalytic Mechanism of CMPAs in Reducing 4-NP

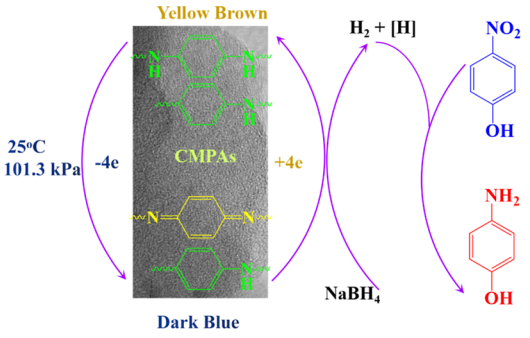

(CMPA-X-Y with higher S_{BET} resulting in enhanced adsorption capacity for both the 4-NP and BH_4^-). The oxidation units in CMPAs were reduced to reduction units in the aqueous solution of $NaBH_4$, as evidenced by the observed color change from dark blue to yellowish brown and the varying rates of color transformation among CMPAs (the shortest time was required for CMPA-3-0.7, which possessed the highest amine group content, Figure S18). H_2 or other [H] active species were released through the decomposition of $NaBH_4$, which subsequently facilitated 4-NP being reduced to 4-AP. Second, the newly generated reduction unit in CMPAs was transported to oxidation units, accompanied by the release of electrons in the presence of O_2, which called oxidation process. This was proven by the color change from a yellowish brown to dark blue. CMPA-3-0.7, with the highest oxidation peak, showed the fastest color change from a yellowish brown to dark blue. Conversely, CMPA-3-1.5, with the highest reduction peak, showed the slowest color change. The oxidation process also can be observed in the well-known blue bottle experiment of methylene blue and red bottle experiments of safranine in an alkaline solution with glucose or VC as reducing agent.

The oxidation process was also feasible from the point of thermodynamics since the electrode potential of the O_2/H_2O pair (φ = 1.23 V) was higher than that of the −N═/−NH pair (φ = −0.8 eV). Therefore, after one such cycle, CMPA-X-Y returned to its original state, showing a self-healing capability. Then, the aforementioned cycle (reduced by $NaBH_4$ and oxidized to its original state by the O_2 in air) was repeated multiple times, resulting in a continuous and stable catalytic system. To indirectly demonstrate that the newly generated reduction unit in CMPAs can be transported to oxidation units in the presence of air, the reduction reaction of 4-NP under air-free conditions was conducted. The outcomes showed that the

https://doi.org/10.1021/acsomega.3c07891
ACS Omega 2024, 9, 11431−11442

catalytic reduction efficiency of CMPA-3-0.7 decreased significantly (K = 4.80 s^{-1} g^{-1}, k_{app} = 0.00012 s^{-1} vs K = 141.32 s^{-1} g^{-1}, k_{app} = 0.00353 s^{-1} for that under air) (Table 2). When 4-NP catalytic reduction was conducted with the air not being removed, it completed in 18 min (Figure 4B). However, when the air in the catalytic reduction system was removed, only a conversion of 34.58% was achieved even after a reaction time of 60 min (Figure S21). This observation suggested that the oxidation process for the newly generated reduction unit in CMPAs was impeded in the absence of air, thereby preventing complete recovery of catalyst to its initial state and ultimately leading to a significant decline in catalytic efficiency for 4-NP reduction.

The special self-healing properties of CMPA-X-Y were further proved by the oxidation of reduced CMPAs in air along with a color transition from yellowish brown to dark blue when the reduced CMPAs was separated from the 4-NP reduction system and the similar XPS N 1s high resolution spectra of CMPA-3-0.7 before and after the dynamic experiment. Figure S22 clearly shows that after 234 min of dynamic catalytic reduction, the molar ratios of the reduction unit (94.74%) and oxidation unit (5.26%) showed only a marginal deviation from those of the parent CMPA-3-0.7 before the reaction (94.85% reduction unit molar ratio and 5.15% oxidation unit molar ratio). Moreover, nitrogen adsorption−desorption characterization also proved that after catalysis, the pore structure of CMPA-3-0.7 was almost the same as that before catalysis (849 m^2/g of S_{BET}, 416 m^2/g of S_{micro}, 0.177 cm^3/g of V_{micro} and 1.162 cm^3/g of V_{tot} vs 870 m^2/g of S_{BET}, 432 m^2/g of S_{micro}, 0.167 cm^3/g of V_{micro} and 1.149 cm^3/g of V_{tot}), indicating the special self-healing properties of CMPA-X-Y in the 4-NP reduction process (Table 1 and Figure S23) and the excellent catalytic stability. Based on the above discussion, the high catalytic efficiency and stability of CMPAs were attributed to the following factors: (1) the 3D structure with an abundance of coexisting micro/mesopores provided more active centers and a larger S_{BET}. This promoted the adsorption of BH_4^- and 4-NP ions and facilitated electron transfer during reduction; (2) the flexible and reversible redox transition of CMPAs allowed the 4-NP reduction reaction to proceed continuously; and (3) the self-healing CMPAs structure ensured the durability of the catalyst.

CONCLUSIONS

Here, a series of CMPAs with a high reduction degree and S_{BET} were synthesized through the BH coupling reaction mechanism, which were subsequently employed for catalytically reducing 4-NP. Among them, CMPA-3-0.7, synthesized with 4,4′-diaminodiphenylamine as the linker and a 0.7:1 molar ratio of linker to core, demonstrated remarkable S_{BET}/reduction degree and exhibited the most elevated activity parameters, apparent rate constants, as well as cycling stability when employed in catalytically reducing 4-NP. Its catalytic reduction performance was comparable to or even better than certain metal catalysts. The catalytic performance of CMPAs was primarily correlated to the reduction degree and S_{BET}. The higher the reduction degree and S_{BET} of CMPAs are, the higher the catalytic reduction activity. During the reaction, CMPAs underwent a reversible redox transformation, which endowed them with self-healing capabilities and ensured a continuous and stable 4-NP reduction reaction system. The combination of a 3D conjugated microporous structure and flexible/reversible redox transition of CMPAs led to a remarkable efficiency in reducing 4-NP to 4-AP. The remarkable catalytic reduction performance, cyclic stability, combined with the structural self-healing properties of CMPAs, give the catalyst practical application prospects for treating 4-NP wastewater. Furthermore, utilizing them to catalytic biomass conversion is ongoing.

ASSOCIATED CONTENT

Supporting Information

The Supporting Information is available free of charge at https://pubs.acs.org/doi/10.1021/acsomega.3c07891.

UV−vis spectra of 4-NP reduction with spherical PANI/fibrous PANI/bulk PANI/eHA@PANI/CMPAs/Pd-$(dba)_2$ as catalysts and without catalyst; solid UV−vis/FTIR/XPS spectra, the −NH−/=N− content, powder XRD patterns, TGA curve, SEM/TEM images, N_2 adsorption−desorption isotherm and pore size distribution of CMPAs; correlations of C_t/C_0 and $\ln(C_t/C_0)$ vs reaction time t in the 4-NP reduction with $Pd(dba)_2$ as catalyst and with CMPA-3-0.7 as a catalyst in the absence of air; ^1H NMR spectrum of the reaction products for 4-NP reduction with CMPA-3-0.7 as catalyst; HPLC of 4-AP, 4-NP and reaction products for reducing 4-NP; dynamic catalytic reduction of eHA@PANI; the photo images of CMPA-3-0.7 during and after reaction and the color change of CMPA-3-Y after adding $NaBH_4$ aqueous solution; UV−vis spectra of 4-NP/4-AP adsorption with CMPAs as adsorbents; XPS N 1s high resolution spectra, nitrogen adsorption−desorption isotherm/pore size distribution of CMPA-3-0.7 before and after the dynamic experiment (PDF)

AUTHOR INFORMATION

Corresponding Author

Cuiping Li − *School of Chemical Science and Technology, Yunnan University, Kunming 650500, China*; orcid.org/0000-0002-2452-7320; Email: licp830@iccas.ac.cn

Authors

Weiming Gao − *School of Materials and Energy, Yunnan University, Kunming 650500, China*

Dingwu Jiang − *School of Chemical Science and Technology, Yunnan University, Kunming 650500, China*

Yiming Zhang − *School of Chemical Science and Technology, Yunnan University, Kunming 650500, China*

Yao Li − *School of Chemical Science and Technology, Yunnan University, Kunming 650500, China*

Zhilong Xu − *School of Chemical Science and Technology, Yunnan University, Kunming 650500, China*

Runxi Han − *School of Chemical Science and Technology, Yunnan University, Kunming 650500, China*

Hao Tian − *School of Chemical Science and Technology, Yunnan University, Kunming 650500, China*

Hufei Dai − *School of Chemical Science and Technology, Yunnan University, Kunming 650500, China*

Qijing Lu − *School of Chemical Science and Technology, Yunnan University, Kunming 650500, China*

Complete contact information is available at: https://pubs.acs.org/10.1021/acsomega.3c07891

Notes

The authors declare no competing financial interest.

https://doi.org/10.1021/acsomega.3c07891
ACS Omega 2024, 9, 11431−11442

■ ACKNOWLEDGMENTS

We thank the National Natural Science Foundation of China (nos. 51863022, 51563023, 51003091), the Program for Middle-Young Science and Technology Leader Reserve Talents of Yunnan Province (2019HB117), the Program for Youth Top Talent of Yunnan Province Ten Thousand Talents, the Program for Excellent Young Talents (YNWR-QNBJ-2018-096), and Yunnan University's Research Innovation Fund (no. WX069051) for their financial support.

■ REFERENCES

(1) Zhao, H.; Kong, C.-H. Enhanced Removal of *p*-Nitrophenol in a Microbial Fuel Cell after Long-Term Operation and the Catabolic Versatility of Its Microbial Community. *Chem. Eng. J.* **2018**, *339*, 424−431.

(2) Balasubramanian, P.; Balamurugan, T. S. T.; Chen, S.-M.; Chen, T.-W. Simplistic Synthesis of Ultrafine $CoMnO_3$ Nanosheets: An Excellent Electrocatalyst for Highly Sensitive Detection of Toxic 4-Nitrophenol in Environmental Water Samples. *J. Hazard. Mater.* **2019**, *361*, 123−133.

(3) Sharma, A. K.; Mehara, P.; Das, P. Recent Advances in Supported Bimetallic Pd-Au Catalysts: Development and Applications in Organic Synthesis with Focused Catalytic Action Study. *ACS Catal.* **2022**, *12*, 6672−6701.

(4) Qin, L.; Zeng, Z.; Zeng, G.; Lai, C.; Duan, A.; Xiao, R.; Huang, D.; Fu, Y.; Yi, H.; Li, B.; Liu, X.; Liu, S.; Zhang, M.; Jiang, D. Cooperative Catalytic Performance of Bimetallic Ni-Au Nanocatalyst for Highly Efficient Hydrogenation of Nitroaromatics and Corresponding Mechanism Insight. *Appl. Catal., B* **2019**, *259*, 118035.

(5) Xiong, Z.; Zhang, H.; Zhang, W.; Lai, B.; Yao, G. Removal of nitrophenols and their derivatives by chemical redox: A review. *Chem. Eng. J.* **2019**, *359*, 13−31.

(6) Arora, P. K.; Srivastava, A.; Singh, V. P. Bacterial Degradation of Nitrophenols and Their Derivatives. *J. Hazard. Mater.* **2014**, *266*, 42−59.

(7) Chang, Q.; Xu, W.; Li, N.; Xue, C.; Wang, Y.; Li, Y.; Wang, H.; Yang, J.; Hu, S. Dynamic Restructuring of Carbon Dots/Copper Oxide Supported on Mesoporous Hydroxyapatite Brings Exceptional Catalytic Activity in the Reduction of 4-Nitrophenol. *Appl. Catal., B* **2020**, *263*, 118299.

(8) Yan, Z.; Fu, L.; Zuo, X.; Yang, H. Green Assembly of Stable and Uniform Silver Nanoparticles on 2D Silica Nanosheets for Catalytic Reduction of 4-Nitrophenol. *Appl. Catal., B* **2018**, *226*, 23−30.

(9) Wang, H.; Shi, F.; Pu, M.; Lei, M. Theoretical Study on Nitrobenzene Hydrogenation by N-Doped Carbon-Supported Late Transition Metal Single-Atom Catalysts. *ACS Catal.* **2022**, *12*, 11518−11529.

(10) Gao, M.; Wang, L.; Yang, Y.; Sun, Y.; Zhao, X.; Wan, Y. Metal and Metal Oxide Supported on Ordered Mesoporous Carbon as Heterogeneous Catalysts. *ACS Catal.* **2023**, *13*, 4060−4090.

(11) Yan, Q.; Wang, X.; Feng, J.; Mei, L.; Wang, A. Simple Fabrication of Bimetallic Platinum-Rhodium Alloyed Nano-Multipods: A Highly Effective and Recyclable Catalyst for Reduction of 4-Nitrophenol and Rhodamine B. *J. Colloid Interface Sci.* **2021**, *582*, 701−710.

(12) Li, Y.; Quan, X.; Hu, C.; Li, C. Effective Catalytic Reduction of 4-Nitrophenol to 4-Aminophenol over Etched Halloysite Nanotubes@*a*-$Ni(OH)_2$. *ACS Appl. Energy Mater.* **2020**, *3*, 4756−4766.

(13) Zhou, Q.; Shi, G. Conducting Polymer-Based Catalysts. *J. Am. Chem. Soc.* **2016**, *138*, 2868−2876.

(14) Quan, X.; Li, Y.; Gu, H.; Hu, C.; Zhang, Y.; Li, Y.; Gao, W.; Li, C. Sulfonated Polydivinylbenzene Bamboo-Like Nanotube Stabilized Pickering Emulsion for Effective Oxidation of Olefins to 1,2-Diol. *J. Colloid Interface Sci.* **2022**, *606*, 158−166.

(15) Huang, H.; Liu, Y.; Lee, S. T.; Kang, Z. Polymer (Polyanilines) Nanoparticles: A Superior Catalyst for Hydrocarbon Selective Oxidation. *J. Mater. Chem.* **2012**, *22*, 337−340.

(16) Zhou, T.; Zhao, Y.; Han, W.; Xie, H.; Li, C.; Yuan, M. Enhanced Solvent-Free Selective Oxidation of Cyclohexene to 1,2-Cyclohexanediol by Polyaniline@Halloysite Nanotubes. *J. Mater. Chem. A* **2017**, *5*, 18230−18241.

(17) Zhu, L.; Dai, J.; Liu, M.; Tang, D.; Liu, S.; Hu, C. Formyl Modified Polyaniline for the Catalytic Dehydration of Fructose to 5-Hydroxymethylfurfural. *ChemSusChem* **2016**, *9*, 2174−2181.

(18) Dai, J.; Zhu, L.; Tang, D.; Fu, X.; Tang, J.; Guo, X.; Hu, C. Sulfonated Polyaniline as a Solid Organocatalyst for Dehydration of Fructose into 5-Hydroxymethylfurfural. *Green Chem.* **2017**, *19*, 1932−1939.

(19) Zhou, T.; Li, C.; Jin, H.; Lian, Y.; Han, W. Effective Adsorption/Reduction of Cr(VI) Oxyanion by Halloysite@Polyaniline Hybrid Nanotubes. *ACS Appl. Mater. Interfaces* **2017**, *9*, 6030−6043.

(20) Mondal, S.; Mondal, J.; Bhaumik, A. Sulfonated Porous Polymeric Nanofibers as an Efficient Solid Acid Catalyst for the Production of 5-Hydroxymethylfurfural from Biomass. *ChemCatChem* **2015**, *7*, 3570−3578.

(21) Bhanja, P.; Palui, A.; Chatterjee, S.; Kaneti, Y. V.; Na, J.; Sugahara, Y.; Bhaumik, A.; Yamauchi, Y. Crystalline Porous Organic Polymer Bearing -SO_3H Functionality for High Proton Conductivity. *ACS Sustainable Chem. Eng.* **2020**, *8*, 2423−2432.

(22) Ruiz-Castillo, P.; Buchwald, S. L. Applications of Palladium-Catalyzed C-N Cross-Coupling Reactions. *Chem. Rev.* **2016**, *116*, 12564−12649.

(23) Liao, Y.; Weber, J.; Faul, C. F. J. Conjugated Microporous Polytriphenylamine Networks. *Chem. Commun.* **2014**, *50*, 8002−8005.

(24) Liao, Y.; Weber, J.; Mills, B. M.; Ren, Z.; Faul, C. F. J. Highly Efficient and Reversible Iodine Capture in Hexaphenylbenzene-Based Conjugated Microporous Polymers. *Macromolecules* **2016**, *49*, 6322−6333.

(25) Chen, J.; Yan, W.; Townsend, E. J.; Feng, J.; Pan, L.; Del Angel Hernandez, V.; Faul, C. F. J. Tunable Surface Area, Porosity, and Function in Conjugated Microporous Polymers. *Angew. Chem., Int. Ed.* **2019**, *58*, 11715−11719.

(26) Chen, J.; Qiu, T.; Yan, W.; Faul, C. F. J. Exploiting Hansen Solubility Parameters to Tune Porosity and Function in Conjugated Microporous Polymers. *J. Mater. Chem. A* **2020**, *8*, 22657−22665.

(27) Chen, J.; Wang, Y.; Ye, C.; Lyu, W.; Zhu, J.; Yan, W.; Qiu, T. Self-Reducible Conjugated Microporous Polyaniline for Long-Term Selective Cr (VI) Detoxication Driven by Tunable Pore Dimension. *ACS Appl. Mater. Interfaces* **2020**, *12*, 28681−28691.

(28) Chaoui, N.; Trunk, M.; Dawson, R.; Schmidt, J.; Thomas, A. Trends and Challenges for Microporous Polymers. *Chem. Soc. Rev.* **2017**, *46*, 3302−3321.

(29) Liao, Y.; Cheng, Z.; Zuo, W.; Thomas, A.; Faul, C. F. J. Nitrogen-Rich Conjugated Microporous Polymers: Facile Synthesis, Efficient Gas Storage, and Heterogeneous Catalysis. *ACS Appl. Mater. Interfaces* **2017**, *9*, 38390−38400.

(30) Chen, X.; Wang, Y.; Wang, J.; Liu, J.; Sun, S.; Zhu, L.; Ma, Q.; Zhu, N.; Wang, X.; Chen, J.; Yan, W. A COF-Like Conductive Conjugated Microporous Poly(aniline) Serving as a Current Collector Modifier for High-Performance Li-S Batteries. *J. Mater. Chem. A* **2022**, *10*, 1359−1368.

(31) Lyu, W.; Zhang, W.; Liu, H.; Liu, Y.; Zuo, H.; Yan, C.; Faul, C. F. J.; Thomas, A.; Zhu, M.; Liao, Y. Conjugated Microporous Polymer Network Grafted Carbon Nanotube Fibers with Tunable Redox Activity for Efficient Flexible Wearable Energy Storage. *Chem. Mater.* **2020**, *32*, 8276−8285.

(32) Lou, X.; Chen, J.; Xiong, Z.; Tang, D.; Chen, X.; Chen, S.; Dong, R.; Ye, C.; Qiu, T. Porosity Design on Conjugated Microporous Poly(aniline)s for Exceptional Mercury (II) Removal. *ACS Appl. Mater. Interfaces* **2021**, *13*, 61653−61660.

(33) Wang, S.; Xiao, Z.; Ma, X.; Zhao, Z.; Guo, D.; Chen, Y.; Zhai, S.; An, Q.; Yang, D. Hard Template-Induced Internal Solidification Synthesis of Cu NPs-Supported Glutaraldehyde-Crosslinked Poly-

https://doi.org/10.1021/acsomega.3c07891
ACS Omega 2024, 9, 11431−11442

ethyleneimine-Modified Calcium Alginate Beads with Enhanced Catalytic Activity. *Appl. Catal., A* **2018**, *568*, 105−113.
(34) Albuquerque, J. E.; Mattoso, L. H. C.; Balogh, D. T.; Faria, R. M.; Masters, J. G.; MacDiarmid, A. G. A Simple Method to Estimate the Oxidation State of Polyanilines. *Synth. Met.* **2000**, *113*, 19−22.
(35) Govindaraj, Y.; Parida, S. Autogenous Chemical and Structural Transition and the Wettability of Electropolymerized PANI surface. *Appl. Surf. Sci.* **2019**, *481*, 174−183.
(36) Golczak, S.; Kanciurzewska, A.; Fahlman, M.; Langer, K.; Langer, J. Comparative XPS Surface Study of Polyaniline Thin Films. *Solid State Ionics* **2008**, *179*, 2234−2239.
(37) Zhao, Y.; Li, Y.; Quan, X.; Li, C. Facile Preparation of Etched Halloysite@Polyaniline Nanorods and Their Enhanced Electrochemical Capacitance Performance. *Electrochim. Acta* **2019**, *321*, 134715.
(38) Li, C.; Wang, J.; Guo, H.; Ding, S. Low Temperature Synthesis of Polyaniline-Crystalline TiO_2-Halloysite Composite Nanotubes with Enhanced Visible Light Photocatalytic Activity. *J. Colloid Interface Sci.* **2015**, *458*, 1−13.
(39) Li, H.; Li, J.; Thomas, A.; Liao, Y. Ultra-High Surface Area Nitrogen-Doped Carbon Aerogels Derived from a Schiff-Base Porous Organic Polymer Aerogel for CO_2 Storage and Supercapacitors. *Adv. Funct. Mater.* **2019**, *29*, 1−9.
(40) Jiang, J. X.; Su, F.; Trewin, A.; Wood, C. D.; Campbell, N. L.; Niu, H.; Dickinson, C.; Ganin, A. Y.; Rosseinsky, M. J.; Khimyak, Y. Z.; Cooper, A. I. Conjugated Microporous Poly(aryleneethynylene) Networks. *Angew. Chem., Int. Ed.* **2007**, *46*, 8574−8578.
(41) Jiang, D. B.; Liu, X.; Yuan, Y.; Feng, L.; Ji, J.; Wang, J.; Losic, D.; Yao, H.-C.; Zhang, Y. X. Biotemplated Top-Down Assembly of Hybrid Ni Nanoparticles/N Doping Carbon on Diatomite for Enhanced Catalytic Reduction of 4-Nitrophenol. *Chem. Eng. J.* **2020**, *383*, 123156.
(42) Wang, N.; Wen, Q.; Liu, L.; Xu, J.; Zheng, J.; Yue, M.; Asiri, A. M.; Marwani, H. M.; Zhang, M. One Dimensional Hierarchical Nanoflakes with Nickel-Immobilization for High Performance Catalysis and Histidine-Rich Protein Adsorption. *Dalton Trans.* **2019**, *48*, 11308−11316.
(43) Ding, L.; Zhang, M.; Zhang, Y.; Yang, J.; Zheng, J.; Xu, J. A Type of Raspberry-Like Silica Composite with Tunable Nickel Nanoparticles Coverage towards Nanocatalysis and Protein Adsorption. *Green Chem.* **2016**, *18*, 6282−6290.
(44) Guo, P.; Tang, L.; Tang, J.; Zeng, G.; Huang, B.; Dong, H.; Zhang, Y.; Zhou, Y.; Deng, Y.; Ma, L.; Tan, S. Catalytic Reduction-Adsorption for Removal of *p*-Nitrophenol and Its Conversion *p*-Aminophenol from Water by Gold Nanoparticles Supported on Oxidized Mesoporous Carbon. *J. Colloid Interface Sci.* **2016**, *469*, 78−85.
(45) Lv, Z.-S.; Zhu, X.-Y.; Meng, H.-B.; Feng, J.-J.; Wang, A.-J. One-Pot Synthesis of Highly Branched Pt@Ag Core-Shell Nanoparticles as a Recyclable Catalyst with Dramatically Boosting the Catalytic Performance for 4-Nitrophenol Reduction. *J. Colloid Interface Sci.* **2019**, *538*, 349−356.
(46) Revathy, T. A.; Dhanapal, K.; Dhanavel, S.; Narayanan, V.; Stephen, A. Pulsed Electrodeposited Dendritic Pd-Ni Alloy as a Magnetically Recoverable Nanocatalyst for the Hydrogenation of 4-Nitrophenol. *J. Alloys Compd.* **2018**, *735*, 1703−1711.

https://doi.org/10.1021/acsomega.3c07891
ACS Omega 2024, 9, 11431−11442